



## Effect of the microstructural properties of copper on corrosion performance

Tadeja Kosec, Jure Voglar, Petra Močnik & Andraž Legat

To cite this article: Tadeja Kosec, Jure Voglar, Petra Močnik & Andraž Legat (2021) Effect of the microstructural properties of copper on corrosion performance, Corrosion Engineering, Science and Technology, 56:8, 728-735, DOI: [10.1080/1478422X.2021.1947942](https://doi.org/10.1080/1478422X.2021.1947942)

To link to this article: <https://doi.org/10.1080/1478422X.2021.1947942>



© 2021 The Author(s). Published by Informa UK Limited, trading as Taylor & Francis Group



Published online: 14 Jul 2021.



Submit your article to this journal [↗](#)



Article views: 1183



View related articles [↗](#)



View Crossmark data [↗](#)

## Effect of the microstructural properties of copper on corrosion performance

Tadeja Kosec, Jure Voglar, Petra Močnik and Andraž Legat

Slovenian National Building and Civil Engineering Institute, Ljubljana, Slovenia

### ABSTRACT

The aim of the study was to define the influence of microstructural properties on the electrochemical properties of copper in four different forms: copper in sheet form, copper doped with phosphorus, electroplated copper and copper wire. Open circuit potential and polarization resistance measurements were carried out in order to determine the electrochemical properties and corrosion rates of copper in 0.1 M NaCl solution in oxic conditions at ambient temperature. Statistical evaluation of the electrochemical data was performed in order to differentiate between the various forms of copper samples. Microstructural and electrochemical investigations were combined with electron microscopy and Raman analysis of the corrosion products after immersion of the copper samples in a 0.1 M NaCl solution for 30 days. The various morphologies of copper corrosion products were identified and analyzed by Raman spectroscopy for the various forms of copper.

### ARTICLE HISTORY

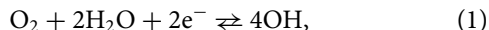
Received 8 April 2021  
Accepted 19 June 2021

### KEYWORDS

Copper; microstructure;  
electrochemical properties;  
corrosion monitoring;  
corrosion products

### Introduction

The electrochemical behaviour of copper in aerated chloride solutions is well documented [1–5]. Corrosion properties vary according to pH and the chloride ion concentration. In a neutral aerated chloride solution it is believed that the cathodic reaction for copper is the reduction of oxygen, according to the following reaction:



while the anodic reaction is copper oxidation to Cu (I), which can be present as either  $\text{CuOH}_{(\text{ads})}$  or  $\text{Cu}_2\text{O}$  during long-term exposure to chloride solution [2,3]. Chloride ions can substitute the hydroxyl ions.

Electrochemical investigation showed that, at higher concentrations of chloride and/or higher anodic potentials,  $\text{CuCl}$  dissolves through the formation of  $\text{CuCl}_2$ , which is stable, soluble and stops the protective behaviour of the copper. The dissolution of  $\text{CuCl}_2$  is mass controlled [3,4]. The copper chloride complex may either dissolve away, or it can oxidise to form  $\text{Cu}^{2+}$ , as was confirmed at higher anodic potentials [3,5]. Similar behaviour has been reported in high copper alloys such as copper–zinc and copper–nickel, with studies confirming a similarity to the behaviour of pure copper [6,7].

Recent studies of copper have been connected to the use of copper for canisters, backfilled with compacted bentonite clay, used to place spent nuclear fuel in geologic repositories. These are currently in place in both, the Scandinavian and Canadian high-level radioactive waste disposal programs, with the lifetime of the Cu container designed to be above  $10^6$  years [8,9]. A container made of Cu provides an absolute barrier to the release of radionuclides, so its corrosion has been studied extensively [10–16]. A number of environmental parameters can affect the corrosion behaviour of the copper container here, namely the solution chemistry (the presence of chlorides, sulphates, and bicarbonates),

temperature and heat transfer, saturation of the surrounding bentonite, and the rate of consumption of the trapped oxygen. Following the consumption of oxygen, a supply of dissolved  $\text{SH}^-$  to the copper surface will be detrimental [8]. Consequently, the corrosion of Cu in sulphide systems under anoxic conditions has been studied extensively [12–16]. Lately, many studies have been devoted to understanding the effect of different anion concentrations on the adsorption of  $\text{HS}^-$  to copper under anoxic conditions [14,15]. It was shown that, in anoxic conditions, passivity is very much dependent on the solution chemistry and temperature [16]. It was, however, shown, that even small amounts of sulphide influenced the corrosion of copper during the early oxic repository period [17].

The effects of long-term exposure of copper to various environments can be evaluated using multiple non-destructive corrosion monitoring techniques. One possible technique for monitoring corrosion is the use of an electrical resistance (ER) probe [18–20]. Electrochemical impedance spectroscopy (EIS) measurements have also been performed during long-term exposure of copper to bentonite, with ER probes serving as working electrodes for the EIS [21]. Another possible method is measuring the spatio-temporal distribution of currents using coupled multi-electrode array (CMEA) sensors [22,23]. Copper CMEAs have been used in studies investigating copper pitting in drinking water, and for the long-term monitoring of copper exposed to bentonite in an oxic environment [24,23].

Copper can be delivered in many forms e.g. wires, sheets, or rods, with each of these copper products having undergone different manufacturing processes. When producing ER sensors from electroplated copper, and CMEA sensors from copper wires, it is important to be aware that the manufacturing history of a given material can affect its microstructural properties, which may subsequently impact both the mechanical and electrochemical properties of the final

product. The main aim of this paper is therefore to study the effect of the microstructure on corrosion properties in different forms of copper.

It has been reported that, in a 0.1 M NaOH solution, the passive film of Cu(I) oxide is thicker at grain boundaries than on the grains, and that no metal is preferentially consumed by transient dissolution at the grain boundaries [25,26]. Martinez-Lombardia et al. investigated grain-dependent corrosion on microcrystalline copper in a 10 mM HCl aqueous solution and reported the dependence of grain orientation on corrosion [27]. No other relevant reports were found regarding the effect of microstructure on the corrosion behaviour of copper.

The aim of this study is to investigate the properties of four different forms of high-purity copper. The microstructural properties were studied and their effects on electrochemical properties were investigated in an aerated 0.1 M NaCl solution. The corrosion products that developed on different copper electrodes following immersion in an 0.1 M NaCl aqueous solution for 30 days were examined by EDS and Raman spectroscopy.

## Materials and methods

Samples of copper in four different forms were supplied by various manufacturers:

- a disc ( $\theta = 15$  mm) cut from 2-mm thick Cu-sheet (oxygen-free, high thermal conductivity of 99.95%, cold rolled and soft annealed) (Cu-sheet); Goodfellow, Huntingdon, England, UK.
- Phosphorous doped (62 ppm), 99.99% oxygen-free copper discs of 6 mm diameter and 4 mm height (Cu-OF); Swedish Nuclear Fuel and Waste Management Co. (SKB), Stockholm, Sweden.
- Electroplated copper (99.95%, 25  $\mu$ m thick) on glass-fibre circuit board substrate (Cu-EP), cut into a disc of 15 mm diameter.
- Copper wires from phosphorus-deoxidised copper (99.90%, 1.4 mm diameter wires, cold drawn and soft annealed at 200 °C).

Electroplated copper (Cu-EP) was used to fabricate copper ER sensors for monitoring corrosion. The use of such copper sensors for the long-term monitoring of corrosion has been reported in our previous studies [19,17,28].

Copper wires (Cu-wire) were used to fabricate a CMEA consisting of 25 wire electrodes assembled into a  $5 \times 5$  matrix in epoxy resin. The exact structure of the array, as well as the

electrical configuration for the measurements, has been described in our previous work [22]. The use of copper CMEA sensors was demonstrated in our study monitoring the corrosion of copper in bentonite slurry over an extended period of time [23].

The samples (i.e. working electrodes) for electrochemical tests in this study were cut from sheet in the form of discs with a diameter of 15 mm (Figure 1(a,c)). In order to remove the oxide film, the samples were ground with 800–2400 grit SiC paper, with the exception of the electroplated copper on printed circuit board, which was used in the state supplied. The samples were ultrasonically cleaned in 96% ethanol for 3 min and then air-dried. For the metallographic investigation, the samples were polished with 1  $\mu$ m  $\text{Al}_2\text{O}_3$  paste and etched with 50 mL distilled water, 50 mL ethanol and 2.5 mg of ferric nitrate. All samples were cleaned in non-denatured 96% ethanol. A Carl Zeiss Axio optical microscope was used to examine the specimens.

In the case of the Cu-sheet and Cu-EP, a three-electrode corrosion cell with a volume of 350  $\text{cm}^3$  was used for electrochemical measurements, with the electrodes embedded in a Teflon holder. The corrosion medium was a 0.1 M NaCl solution with pH 5.9. The grade of chemicals used was p.a. The tests were conducted at room temperature in oxic conditions. In the case of the Cu-wire electrodes in a copper CMEA sensor, four wires were connected into one working electrode, exposing an area of 0.0616  $\text{cm}^2$  (marked with a blue line, as shown in Figure 1(d)). The reference electrode was an Ag/AgCl with 3 M KCl, and the counter electrode a graphite rod (with an exposed area of around 15  $\text{cm}^2$ ). A Gamry Ref 600+ expanded with Gamry framework software was used for data collection. Electrochemical testing was conducted after 1-hour stabilisation at open circuit potential (OCP), followed by linear polarisation measurements at  $\pm 20$  mV vs. OCP at a scan rate of 0.1  $\text{mV s}^{-1}$ . All potentials are reported with respect to the Ag/AgCl scale (0.210 V vs.  $E_{\text{NHE}}$ ), and all values are normalised (Figure 2).

The samples of copper in Cu-sheet, Cu-OF and Cu-EP form were also immersed in a 0.1 M NaCl aqueous solution for 30 days with the intention to study the corrosion products developed after exposure to a corrosive environment. Following immersion, the samples were cleaned with 96% ethanol and then inspected to determine the shape and size of the surface corrosion products. This was done via Field Emission Scanning Electron Microscopy (FE-SEM, Zeiss ULTRA plus, Germany) operated at an accelerating voltage of 20 kV. Raman spectroscopy was applied to identify corrosion products on the copper. The Raman spectra were recorded by means of a Horiba Yvon HR800 spectrometer. The samples were irradiated with a green laser ( $\lambda =$

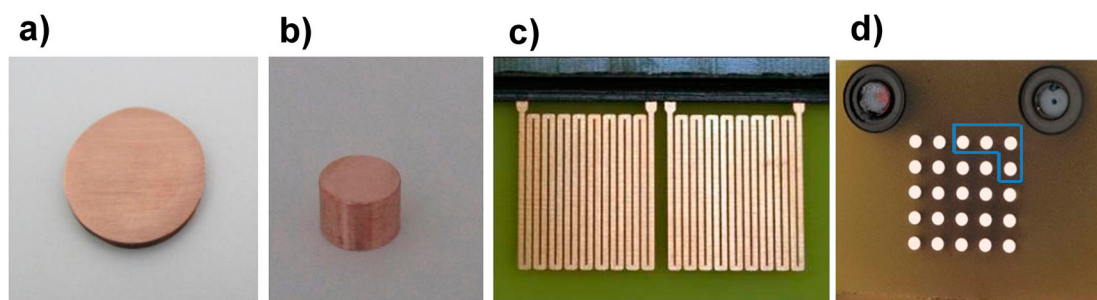
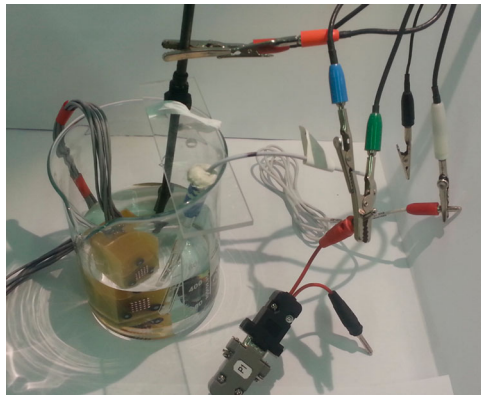


Figure 1. Copper samples: (a) discs cut from 2 mm Cu-sheet, (b) Cu-OF copper, (c) Cu-EP and (d) a  $5 \times 5$  1.4 mm Cu-wire CMEA.



**Figure 2.** Electrochemical testing of 4 of the 25 Cu-wires in a copper multi-electrode array (CMEA) in 0.1 M NaCl solution.

514 nm) at a power of 14 mW. For 50× long distance objective, spot size of a laser was 1,25 μm. Multiple spectra were measured, while only the representative spectra are presented. The scanning range was 50–4000 cm<sup>-1</sup>, or 50–1000 cm<sup>-1</sup> when only cuprite was expected.

## Results and discussion

### Microstructural analysis

The microstructures of the various copper samples were examined and the images are presented in Figure 3. The specific cross sections observed were those which would later be exposed to a corrosive medium during experimental work and/or operation of the sensors.

The 2 mm copper sheet (Cu-sheet) was cold rolled and soft annealed; consequently its α-phase copper crystal grains are very large, ranging between 60 and 80 μm, and are oriented and elongated in the rolling direction (Figure 3

(a)). Alpha phase copper is predicted to be present on the basis of the chemical composition of the copper samples, which all contain at least 99.90 mass.% of copper [29]. The rolling direction was predicted from the shape and orientation of the crystal grains in the sample's microstructure, since the crystal grains of a metallic alloy become elongated in the direction of rolling (the direction of observation). Inclusions of P<sub>2</sub>O<sub>5</sub> were detected in the microstructure of the Cu-sheet, both within the crystal grains and at the crystal grain boundaries.

The crystal grains of the oxygen-free copper (Cu-OF) are very large and the grain boundaries are the most distinguishable. The size of α-phase copper crystal grains varies between 50 and 150 μm. Owing to processing procedures the grains are uniformly oriented in all directions (Figure 3(b)). There are no visible inclusions of either Cu<sub>2</sub>O or P<sub>2</sub>O<sub>5</sub> in the microstructure, as respectively observed under polarised light or in the dark field (images not shown); the small dots that can be seen are impurities arising from the metallographic preparation of the sample.

The electroplated copper (Cu-EP) consists of uniformly oriented α-phase copper crystal grains ranging in size from 5 to 15 μm (Figure 3(c)). The microstructure does not contain phosphorus to deoxidise the metal nor cupric oxide (Cu<sub>2</sub>O) inclusions. The crystal grains of the sample are elongated and oriented in the direction of the electroplating deposition, as observed by inspection of cross-section of the Cu-EP sample (Figure 3(c)).

The copper wire for electrode arrays (Cu-wire) has fine α-phase crystal grains, ranging in size from 10 to 20 μm (Figure 3(d)). Phosphorus oxide (P<sub>2</sub>O<sub>5</sub>) inclusions are present in the microstructure, as confirmed by light-coloured dots observed in the dark field (not shown). The crystal grains are most likely elongated in the drawing direction of the wire, but the longitudinal cross-section of the wire was not observed.

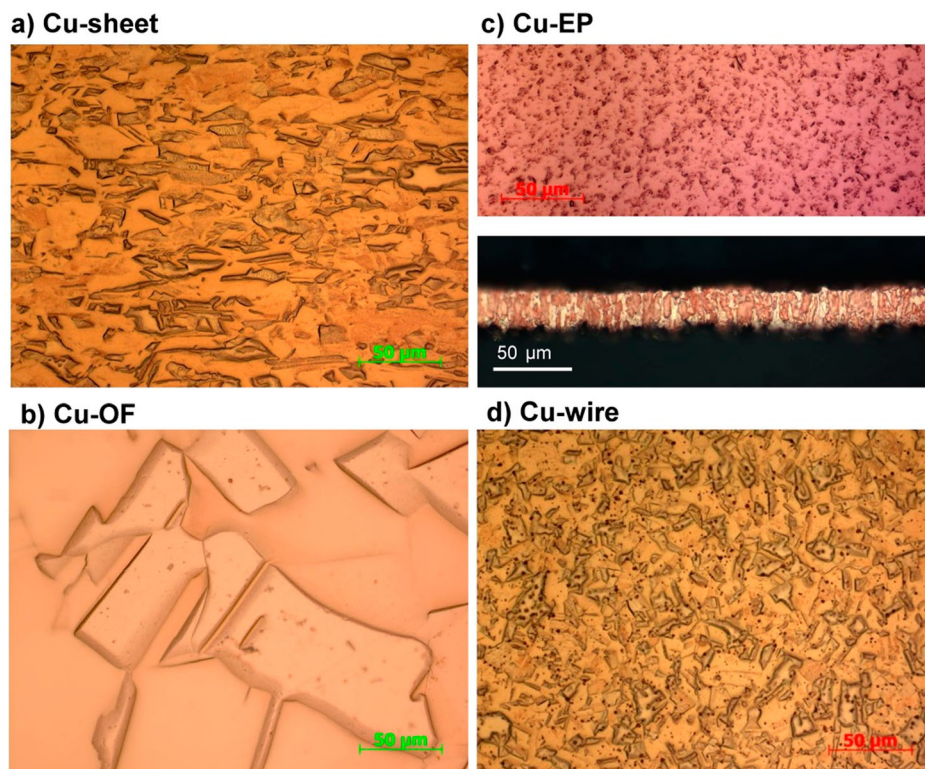


**Figure 3.** Microstructures of the different forms of copper: (a) Cu-sheet (b) Cu-OF (c) Cu-EP in transversal direction and cross-section and (d) Cu-wire.

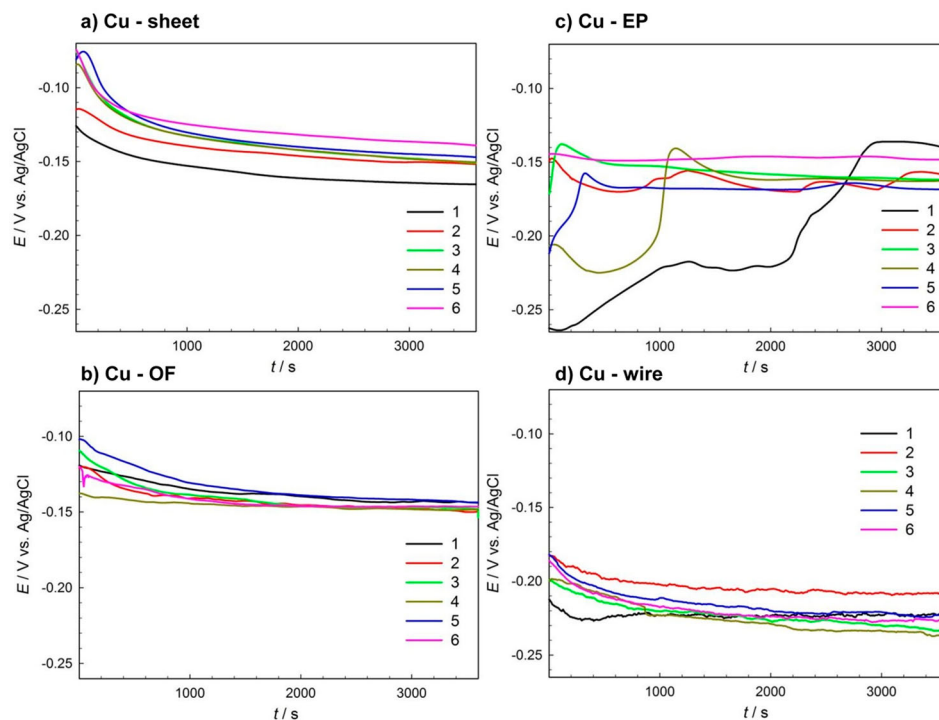


**Figure 4.** Replicate measurements of OCP on (a) Cu-sheet, (b) Cu-OF, (c) Cu-EP and (d) Cu-wire in 0.1 M NaCl

There were no visible inclusions in the microstructure of  $\alpha$ -phase copper crystal grains in the Cu-OF samples, whereas cupric oxide ( $\text{Cu}_2\text{O}$ ) inclusions were observed in the  $\alpha$ -phase copper crystal grains of the Cu-EP. Phosphorus oxide ( $\text{P}_2\text{O}_5$ ) inclusions were observed in the  $\alpha$ -phase copper crystal grains of the Cu-sheet and are present in an even greater abundance in the Cu-wire.

## Electrochemical measurements

### Open circuit potential

OCP of the different copper electrodes was measured six times in a 0.1 M NaCl aqueous solution. Between the replicate measurements, the copper surface was freshly ground and immersed in a fresh solution. In the case of Cu-EP, a new sample was used for each measurement. All OCP measurements are presented in Figure 4, and the results are summarised in Table 1.

In the case of the copper sheet and Cu-OF, the potential at first decreased slightly when exposed to the solution (Figure 4(a,c), Table 1), but in general, it did not vary much with time or between replicate measurements (showing a standard deviation of only 0.005 V). The  $E_{\text{OCP}}$  at 3600 s was  $-0.151$  for the Cu-sheet and  $-0.147$  V for Cu-OF (Table 1).

The initial OCP value of Cu-EP (Figure 4(c)) was more negative by about 50–100 mV upon exposure of the electrode to the solution, then stabilised to a constant value (at

1500 s). The OCP of the Cu-EP sample was  $-0.152$  V, similar to that of the Cu-sheet sample (Table 1).

The OCP measurement of the Cu-wire (Figure 4(d)) was the lowest among all of the measured potentials ( $-0.225$  V at 3600 s).

Variation between replicate measurements of OCP values was greatest in the Cu-EP and Cu-wire.

### Linear polarisation measurements

Each form of copper material was measured six times using the linear polarisation corrosion measurement, using a slow scan rate of  $0.1 \text{ mV s}^{-1}$  to ensure that the real kinetics of the reaction were detected and that the working electrode double layer could adjust to any potential change [30,31]. Linear polarisation measurements for the various copper samples are presented in Figure 5.  $R_p$  values represent the slope of the tangent to the curves where the current is 0. The values of polarisation resistance,  $R_p$ , in  $\Omega \text{ cm}^2$  are presented in Table 2. The corrosion rate values for one and two electrode processes ( $n = 1$  and  $n = 2$ , respectively) are further given in Table 2. The c be discussed later in the text.

Polarisation resistance values,  $R_p$ , are highest in Cu-sheet and electroplated copper (Cu-EP), with respective values of 26.7 and  $36.0 \text{ k}\Omega \text{ cm}^2$  at similar average values of  $E_{\text{OCP}}$ .

$R_p$  values for the phosphorus-doped copper, Cu-OF, are lower, at  $16.4 \text{ k}\Omega \text{ cm}^2$ .

**Table 1.** Electrochemical potential read at the end of the OCP measurement for each type of Cu material.

No	Potential of Cu-sheet/V	Potential of Cu-EP/V	Potential of Cu-OF/V	Potential of Cu-wire/V
1	-0.165	-0.141	-0.144	-0.223
2	-0.152	-0.159	-0.150	-0.208
3	-0.151	-0.162	-0.148	-0.232
4	-0.150	-0.162	-0.149	-0.237
5	-0.147	-0.148	-0.144	-0.223
6	-0.139	-0.137	-0.147	-0.226
Average and standard deviation	$-0.151 \pm 0.008$	$-0.152 \pm 0.01$	$-0.147 \pm 0.003$	$-0.225 \pm 0.01$

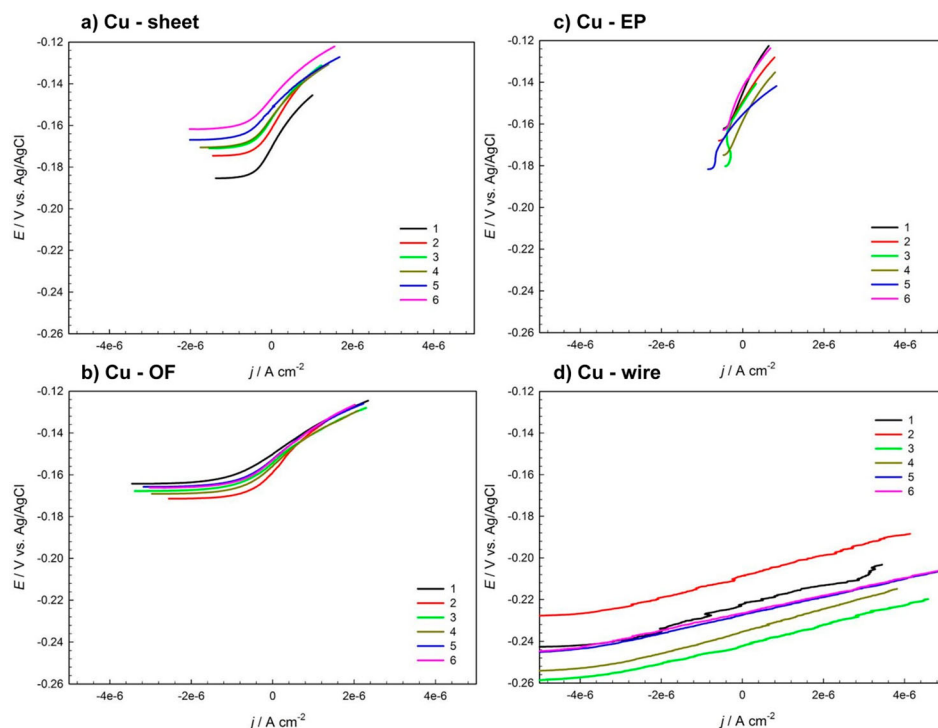


**Figure 5.** Replicate measurements of linear polarisation on (a) Cu-sheet, (b) Cu-OF, (c) Cu-EP and (d) Cu-wire in 0.1 M NaCl.

The average  $R_p$  value for the Cu-wire ( $4.91 \text{ k}\Omega \text{ cm}^2$ ) is lowest of all copper samples with more negative potentials than other copper samples, as can be observed in Figure 5.

Scatter diagrams for each copper sample, showing the variation in polarisation resistance across repetitive measurements, can be seen in Figure 6. In these diagrams, corrosion data are log-normally distributed [31].  $R_p$  values were therefore transformed to log format [32]. It can be seen that the highest variation between measurements is observed in the Cu-EP samples. Although these exhibited the highest  $R_p$  values, this variation could also be owing to the different surface state of the Cu-EP samples, which were prepared by only ultrasonic cleaning, without grinding. A different Cu-EP working electrode was used each time, in as-received state, with the presence of cuprite on the surface, as is the case when using Cu-EP plates for the fabrication of ER sensors, as described in the Materials and Methods section. In addition to the impact of grain size, defects are present in this material, which may also have an effect on the variation between electrochemical results. It is also evident that the lowest  $R_p$  values are observed in the Cu-wire. This could be attributed to the more complex microstructure, which contains the highest percentage of impurities among all the copper samples investigated, as well as the inclusions of phosphorus oxide and the very small size of the crystal grains (Figure 3(d)).

Mean  $R_p$  values of the various copper samples were also compared by means of the Mann–Whitney test [31]. The Mann–Whitney test, which is used when the number of repetitive measurements is small (e.g. six measurements), determined that the polarisation resistance of the Cu-sheet, Cu-EP and Cu-OF samples are similar to one another, while none of the samples are similar to the Cu-wire samples. The results of the Mann–Whitney test are presented in Table 3.

The Mann–Whitney test showed that the  $R_p$  values of the Cu-wire sample (Cu-wire) are lower than all of the other copper samples tested (Cu-sheet, Cu-OF and Cu-EP). Consequently, its corrosion rate, which is inversely proportional to the  $R_p$  value, is the highest of all the copper samples tested.

The corrosion rate, CR, in  $\mu\text{m}/\text{year}$  was then calculated using Faradaýs law [30], as follows:

$$\text{CR} = k \cdot j_{\text{corr}} \cdot W / (d \cdot n), \quad (2)$$

where  $j_{\text{corr}}$  is the corrosion current density in  $\mu\text{A cm}^{-2}$ ,  $k = 3.27 \mu\text{m g} (\mu\text{Acm})^{-1} \text{ year}$ ,  $d$  is the density in  $\text{g cm}^{-3}$ , and  $W$  is the atomic weight equivalent. For pure copper, the density and atomic weight equivalent are  $8.94 \text{ g cm}^{-3}$  and  $63.55$ , respectively.  $n = 2$ , which is the number of electrons required to oxidise an atom.

**Table 2.** Linear polarisation resistance values of replicate measurements on different Cu electrodes alongside the calculated corrosion rate (CR) in  $\mu\text{m}/\text{year}$ .

No	Cu-sheet/ $\text{k}\Omega \text{ cm}^2$	Cu-OF/ $\text{k}\Omega \text{ cm}^2$	Cu-EP/ $\text{k}\Omega \text{ cm}^2$	Cu-wire/ $\text{k}\Omega \text{ cm}^2$
1	33.4	13.0	40.3	5.56
2	32.3	21.3	22.2	5.25
3	27.7	15.8	42.4	4.72
4	25.7	17.3	31.3	5.33
5	19.2	15.5	31.9	4.40
6	21.7	15.5	47.6	4.16
Average and standard deviation	$26.7 \pm 5.7$	$16.4 \pm 2.8$	$36.0 \pm 9.2$	$4.91 \pm 0.56$
CR ( $n = 1$ )	$15 \pm 3$	$26 \pm 4$	$8 \pm 2$	$123 \pm 13$
CR ( $n = 2$ )	$7 \pm 1$	$13 \pm 2$	$4 \pm 1$	$61 \pm 7$

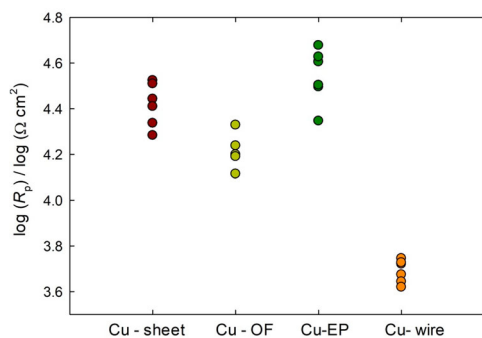


**Figure 6.** Scatter diagram showing the logarithm of the polarisation resistance measured.

**Table 3:** Results of the Mann Whitney test comparing the polarization resistance of the various forms of copper.

	Cu-sheet	Cu-OF	Cu-EP	Cu-wire
Cu-sheet	/	similar	similar	different
Cu-OF	similar	/	similar	different
Cu-EP	similar	similar	/	different
Cu-wire	different	different	different	/

$j_{\text{corr}}$  was calculated from the  $R_p$  values (Table 2):

$$j_{\text{corr}} = \frac{\beta_A \cdot \beta_C}{2.3R_p(\beta_A + \beta_C)}, \quad (3)$$

where  $R_p$  is polarisation resistance in  $\Omega \text{ cm}^2$ ,  $j_{\text{corr}}$  is the corrosion current density in A, and  $\beta_A$  and  $\beta_C$  are Tafel coefficients obtained from Tafel measurements (not shown).

It can be seen from Table 2 that lower  $R_p$  values resulted in higher corrosion rates. Values for corrosion rates are given in the case that cuprite formed ( $n = 1$ ) and when  $\text{Cu}^{2+}$  products formed ( $n = 2$ ).

Taking into account that cuprous oxide was the predominant anodic reaction with  $n = 1$ , as indicated in Table 2, the corrosion rate measured in Cu-sheet, was at  $15 \pm 3 \mu\text{m}/\text{year}$ . The highest corrosion rate was measured in Cu-wires, at  $123 \pm 13 \mu\text{m}/\text{year}$ . The value for Cu-OF, which is copper free from impurities and detected inclusions in the form of  $\text{Cu}_2\text{O}$ , is  $26 \pm 4 \mu\text{m}/\text{year}$ .

The corrosion rate for Cu-EP, however, is the lowest, at  $8 \pm 2 \mu\text{m}/\text{year}$ . As already stated, this low value can be attributed to the surface state of the electroplated electrode. This was not freshly prepared, but tested in an as-received state, meaning that  $\text{Cu}_2\text{O}$  was potentially present during the testing. This was proven by SEM/EDS investigation of the Cu-EP electrode surface before electrochemical testing (not shown), which showed that the surface was, indeed, covered with  $\text{Cu}_2\text{O}$ . Since the as-received state of Cu is typically used in the fabrication of ER sensors, the value obtained for comparison of the copper samples is correct. Sensors fabricated using electroplated printed circuit board (sample Cu-EP) would give a corrosion rate value of  $8 \mu\text{m}/\text{year}$ , and when the corrosion rate needs to be estimated on the Cu-OF sample then it would be underestimated using copper ER sensors. If the sensors fabricated from Cu-wire were used to estimate corrosion rates and then compared to the Cu-OF sample, then the actual corrosion rate of Cu-OF would be lower than that measured by the Cu coupled multi-electrode sensors. The corrosion rate of Cu-OF would be

$26 \mu\text{m}/\text{year}$ , which lies in between the rates for Cu-EP and Cu-wire.

This leads us to the conclusion that using copper sensors fabricated from electroplated copper measures a lower corrosion rate in a 0.1 M NaCl solution than that measured on Cu-OF copper. In the case of Cu-wire and the CMEA sensor, the corrosion rate measured on the CMEA sensor is higher than that of the Cu-OF copper.

This study shows that the microstructural properties of different forms of pure copper significantly influence its corrosion properties, even though the chemical compositions of the materials are extremely similar (minimum 99.90% copper). It is also important to be aware that this work does not address whether the differences in corrosion rate result from differences in microstructure, or from differences in impurity content. Special care should always be taken when estimating the corrosion rates of similar materials, as is shown in this study.

### Analysis of surface corrosion products following long-term immersion

FE-SEM images and Raman spectra of corrosion products formed on the surfaces of the Cu-sheet, Cu-OF and Cu-EP samples after 30 days exposure to a 0.1 M NaCl aqueous solution are presented in Figure 7. Corrosion products on the Cu-wire of a CMEA sensor could not be studied owing to the large size of the sample, meaning that it could not fit into the investigation chamber. The corrosion products non-uniformly cover all the copper surfaces investigated (Figure 7(a-c)). The morphologies of the corrosion products can be seen at a smaller scale in the middle images of Figure 7 (a-c). Observation of the Cu-sheet sample (Figure 7(a)) by the naked eye (photo not shown) points to the possible presence of cuprite, as the surface is mainly reddish-brown, with some patches of green. The corrosion products are in the form of cubic and octahedral structures (Figure 7(a)).

Raman spectra on the Cu-sheet (Figure 7(a)) revealed the presence of both cuprite and atacamite. Cuprite can be confirmed by the strongest bands in the spectrum, positioned at 422, 512 and 642  $\text{cm}^{-1}$ . Several characteristic bands in the Raman spectrum, positioned at 512, 898, 935, 976  $\text{cm}^{-1}$ , and the bands at 2933, 3357 and 3436  $\text{cm}^{-1}$ , further point to the presence of atacamite,  $\text{Cu}_2(\text{OH})_3\text{Cl}$  [33–35]. The presence of tenorite, CuO, was not expected. Furthermore, paratacamite, a polymorph of atacamite, was not anticipated, since paratacamite is a phase more thermodynamically stable over 100 °C at ordinary pressures [36].

Corrosion on the Cu-OF sample (Figure 7(b)) primarily consists of cubic-structured corrosion products across the surface. The Raman spectrum for the Cu-OF (Figure 7(b)) consists of two main features: narrow low frequency bands at 144 and 216  $\text{cm}^{-1}$ , and three broad bands positioned at 419, 536 and 637  $\text{cm}^{-1}$ . The spectrum confirmed the presence of cuprite,  $\text{Cu}_2\text{O}$ , as previously reported [34,35,37]. Raman bands at 898, 935, and 976  $\text{cm}^{-1}$ , in the range from 50 to 1000  $\text{cm}^{-1}$ , were absent, so it can be concluded that atacamite was not present in the Cu-OF sample.

It can be seen from the FE-SEM images that two distinctive corrosion product structures are present on the Cu-EP sample (Figure 7(c)): firstly cubic crystals, and in some areas, these are also covered by a layer of orthorhombic crystals. Both cuprite and atacamite were identified on the

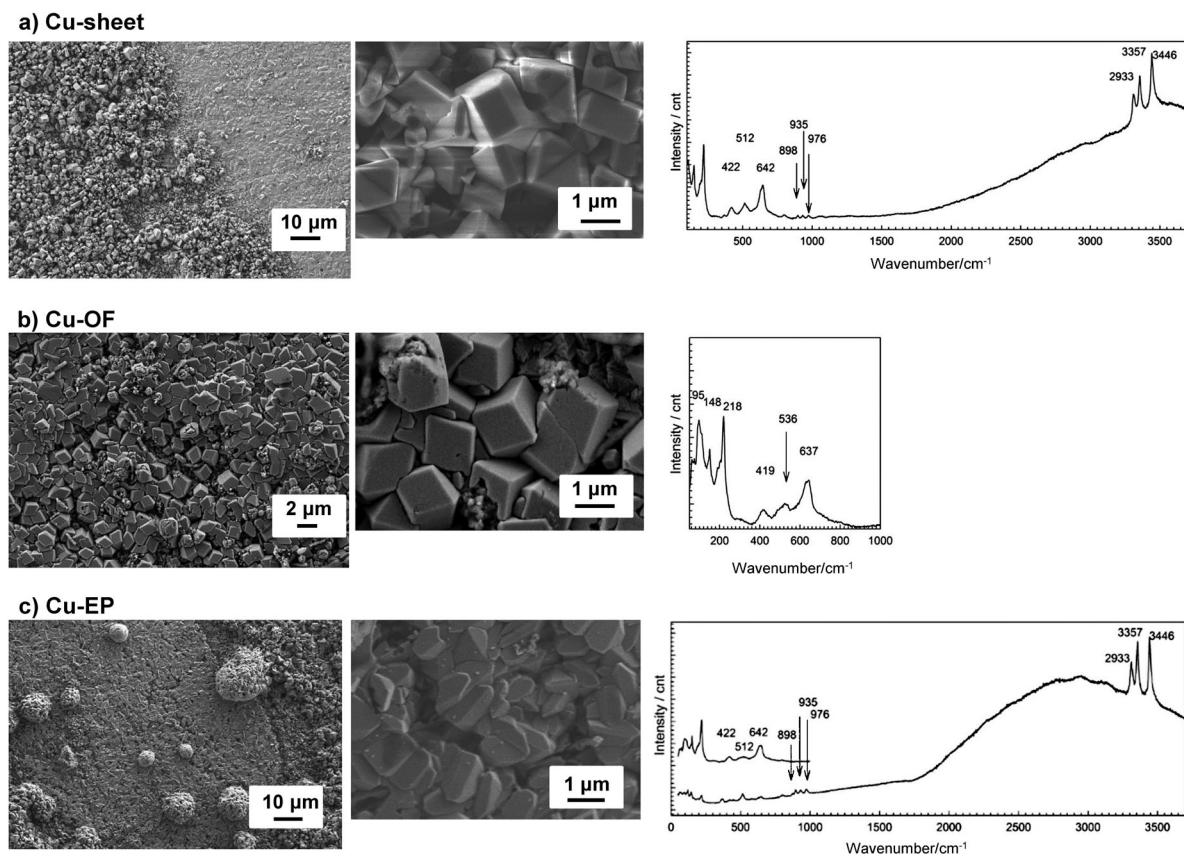


**Figure 7.** FE-SEM images and Raman analysis of corrosion products formed on Cu surfaces after 30 days exposure to the 0.1 M NaCl aqueous solution: (a) Cu-sheet (b), Cu-OF and (c) Cu-EP.

surface of the Cu-EP (Figure 7(c)), similar as to on the Cu-sheet. Cuprite was identified on areas with cubic crystals (the upper Raman spectra in Figure 7(c)), while atacamite was identified on areas with orthorhombic crystals (the lower Raman spectra in Figure 7(c)).

The large crystal grains (175  $\mu\text{m}$  on average) of Cu-OF induced the growth of cuprite crystals, while Raman spectroscopy identified that the corrosion products on copper surfaces with smaller crystal grains (average size smaller than or equal to 75  $\mu\text{m}$ ), i.e. Cu-sheet and Cu-EP, comprised both cuprite and atacamite. No direct correlation can be drawn between the size of crystal grains (as observed by metallographic examination) and the type of corrosion product observed.

The size of selected individual cuprite ( $\text{Cu}_2\text{O}$ ) grains were measured at larger (FE-SEM) magnifications (5000-times to 10000-times) and were determined to be 0.28–1.17  $\mu\text{m}$  on Cu-sheet, between 1.00 and 1.78  $\mu\text{m}$  on Cu-OF, and from 1.32 to 1.48  $\mu\text{m}$  on Cu-EP. No distinctive conclusion can be drawn between the size of the crystal grains, as observed by metallographic examination, and the size of the corrosion products grown at the surface of each of the copper samples.

## Conclusions

Four different forms and grades of copper (99.90% or more) were studied microscopically, electrochemically (in a 0.1 M NaCl aqueous solution, oxic conditions at ambient temperature) and spectroscopically, in order to study the effect of microstructural properties on the corrosion performance of copper. The various forms and grades of copper were chosen in order to assess any differences in their corrosion rates.

- (1) It was shown that the microstructural properties of the various forms of copper differed, both in terms of the size and orientation of crystal grains in the crystal grain lattice, as well as with respect to the presence of  $\text{Cu}_2\text{O}$  and  $\text{P}_2\text{O}_5$  inclusions. The largest crystal grains, sized up to 150  $\mu\text{m}$ , were found in the Cu-OF copper, while Cu-wire and Cu-EP had the smallest crystal grains of size 5–20  $\mu\text{m}$ . Cu-wire contained the largest number of non-metallic inclusions.
- (2) The microstructure affects the electrochemical properties of the different forms of copper. Namely, polarisation resistance changed in accordance with the size of the copper crystal grains. The polarisation resistance, measured on freshly ground copper upon immersion to 0.1 M NaCl after stable OCP was reached, was: for copper with larger crystal grains, sized 100–150  $\mu\text{m}$  ( $16.4 \pm 2.8 \text{ k}\Omega \text{ cm}^2$ ) and it was higher than that of Cu-wire, with crystal grains sized 10–20  $\mu\text{m}$  ( $4.9 \pm 0.6 \text{ k}\Omega \text{ cm}^2$ ).
- (3) Statistical methodology was used in order to differentiate between the corrosion properties of the copper samples. It is essential to test samples with the same (or very similar) chemical compositions yet different microstructures in order to reliably estimate the corrosion rate of copper in different corrosion systems. In our study, the corrosion rate of Cu exposed to 0.1 M NaCl solution varied greatly, from  $123 \pm 13 \mu\text{m}/\text{year}$  for Cu-wire, to  $26 \pm 4 \mu\text{m}/\text{year}$  for Cu-OF,  $15 \pm 3 \mu\text{m}/\text{year}$  for Cu-sheet and  $8 \pm 2 \mu\text{m}/\text{year}$  for Cu-wire.
- (4) Spectroscopic investigations showed differences in the corrosion products after 30 days exposure to a 0.1 M NaCl aqueous solution. Cuprite was found on the Cu-OF sample, which had the largest crystal grains and

minimal inclusions in the microstructure, while cuprite and atacamite were found on Cu-sheet and Cu-EP.

- (5) When comparing corrosion rates estimated using different forms of high-purity copper, it is essential to study the microstructural and electrochemical properties of each form, so that the underestimation or overestimation of copper corrosion rates in a defined corrosive environment is controlled.

## Acknowledgements

The help of Dr. Erika Švara Fabjan with FE-SEM analysis is acknowledged and greatly appreciated. The help of Viljem Kuhar with the work on metallography is acknowledged.

## Disclosure statement

No potential conflict of interest was reported by the author(s).

## Funding

This work was supported by Javna Agencija za Raziskovalno Dejavnost RS: [grant number P2-0273].

## References

- Deslouis C, Tribollet B, Mengolli G, et al. Electrochemical behavior of copper in neutral aerated chloride solution. I. steady state investigation. *J Appl Electrochem*. 1988;18:373–383.
- Millet B, Fiaud C, Hinnen C, et al. A correlation between electrochemical behavior, composition and semiconduction properties of naturally grown oxide films on copper. *Corros Sci*. 1995;37:1903–1918.
- Lee HP, Nobe K. Kinetics and mechanisms of Cu electrodisolution in chloride media. *J Electrochem Soc*. 1986;133:2035–2043.
- Tromans D, Sun R. Anodic polarization behavior of copper in aqueous chloride/benzotriazole solutions. *J Electrochem Soc*. 1998;145:L42–L45.
- Bech-Nielsen G, Jaskula M, Chorkendorff I, et al. The initial behavior of freshly etched copper in moderately acid, aerated chloride solution. *Electrochim Acta*. 2002;47:4279–4290.
- Kosec T, Milošev I, Pihlar B. Benzotriazole as an inhibitor of brass corrosion in chloride solution. *Appl Surf Sci*. 2007;253:8863–8873.
- Kear G, Barker BD, Stokes K, et al. Electrochemical corrosion behavior of 90-10 Cu-Ni alloy in chloride based electrolytes. *J Appl. Electrochem*. 2004;34:659–669.
- Hall DS, Keech PG. An overview of the Canadian corrosion program for the long-term management of nuclear waste. *Corros Eng Sci Techn*. 2017;52:2–5.
- King F, Hall DS, Keech PG. Nature of the near-field environment in a deep geological repository and the implications for the corrosion behaviour of the container. *Corros Eng Sci Techn*. 2017;52:25–30.
- Rosborg B, Pan J. An electrochemical impedance spectroscopy study of copper in a bentonite/saline groundwater environment. *Electrochim Acta*. 2008;53:7556–7564.
- Bojinov M, Betova I, Lilja C. A mechanism of interaction of copper with a deoxygenated neutral aqueous solution. *Corros Sci*. 2010;52:2917–2927.
- Smith JM, Wren JC, Odziemkowski M, et al. The electrochemical response of preoxidized copper in aqueous sulphide solution. *J Electrochem Soc*. 2007;154:C431–C438.
- Smith JM, Qin Z, King F, et al. Sulfide film formation on copper under electrochemical and natural corrosion conditions. *Corrosion*. 2007;63:135–144.
- Chen J, Qin Z, Shoesmith DW. Long-term corrosion of copper in a dilute anaerobic sulfide solution. *Electrochim Acta*. 2011;56:7854–7861.
- Martino T, Chen J, Qin Z, et al. The kinetics of film growth and their influence on the susceptibility to pitting of copper in aqueous sulphide solutions. *Corros Eng Sci Technol*. 2017;52:61–64.
- Qin Z, Daljeet R, Ai M, et al. The active/passive conditions for copper corrosion under nuclear waste repository environment. *Corros Eng Sci Technol*. 2017;52:45–49.
- Kosec T, Qin Z, Chen J, et al. Copper corrosion in bentonite/saline groundwater solution: effects of solution and bentonite chemistry. *Corros Sci*. 2015;90:248–258.
- Rosborg B, Kosec T, Kranjc A, et al. Electrochemical impedance spectroscopy of pure copper exposed in bentonite under oxic conditions. *Electrochim Acta*. 2011;56:7862–7870.
- Rosborg B, Kranjc A, Kuhar V, et al. Corrosion rate of pure copper in an oxic bentonite/saline groundwater environment. *Corros Eng Sci Techn*. 2011;46:148–152.
- Kouril M, Prosek T, Scheffel B, et al. High sensitivity electrical resistance sensors for indoor corrosion monitoring. *Corros Eng Sci Techn*. 2013;48:282–287.
- Kosec T, Kranjc A, Rosborg B, et al. Post examination of copper ER sensors exposed to bentonite. *J Nucl Mat*. 2015;459:306–312.
- Legat A. Monitoring of steel corrosion in concrete by electrode arrays and electrical resistance probes. *Electrochim Acta*. 2007;52:7590–7598.
- Kosec T, Hren M, Legat A. Monitoring copper corrosion in bentonite by means of a coupled multi-electrode array. *Corros Eng Sci Technol*. 2017;52:70–77.
- Budiansky ND, Bocher F, Cong H, et al. Use of coupled multi-electrode arrays to advance the understanding of selected corrosion phenomena. *Corrosion*. 2007;63:537–554.
- Chen H, Maurice V, Klein LH, et al. Grain boundary passivation studied by in situ scanning tunneling microscopy on microcrystalline copper. *J Solid State Electrochem*. 2015;19:3501–3509.
- Chen H, Bettayeb M, Maurice V, et al. Local passivation of metals at grain boundaries: in situ scanning tunneling microscopy study on copper. *Corros Sci*. 2016;111:659–666.
- Martinez-Lombardia E, Maurice V, Lapeire L, et al. In situ scanning tunneling microscopy study of grain-dependent corrosion on microcrystalline copper. *J Phys Chem C*. 2014;118:25421–25428.
- Marja-Aho M, Rajala P, Huttunen-Saarivirta E, et al. Copper corrosion monitoring by electrical resistance probes in anoxic groundwater environment in the presence and absence of sulfate reducing bacteria, sensors & actuators. *A Phys*. 2018;274:252–261.
- Vander Voort GF. Phase identification by selective etching. In: Vander Voort GF, editor. *Applied metallography*. Boston, MA: Springer; 1986:1–19. [https://doi.org/10.1007/978-1-4684-9084-8\\_1](https://doi.org/10.1007/978-1-4684-9084-8_1)
- Scully JR, Silverman DC, Kendig MW. *Electrochemical impedance: analysis and interpretation*. Philadelphia: ASTM; 1993.
- Tait WS. *An introduction to electrochemical corrosion testing for practicing engineers and scientists*. Racine: PairODocs Publications; 1994.
- Siegel S, Castellan NJ. *Nonparametric statistics for the behavioral sciences*. New York: McGraw-Hill; 1988.
- Hayez V, Costa V, Guillaume J, et al. Micro Raman spectroscopy used for the study of corrosion products on copper alloys: study of the chemical composition of artificial patinas used for restoration purposes. *Analyst*. 2005;130:550–556.
- Frost RL, Leverett P, Williams PA, et al. Raman spectroscopy of gerhardtite at 298 and 77 K. *J Raman Spectrosc*. 2004;35:991–996.
- Marušić K, Otmačić-Čurković H, Horvat-Kurbegović Š, et al. Comparative studies of chemical and electrochemical preparation of artificial bronze patinas and their protection by corrosion inhibitor. *Elsevier*. 2009;54:7106–7113.
- Sharkey JB, Lewin SZ. Conditions governing the formation of atacamite and paratacamite. *Am Mineral*. 1971;56:179–192.
- Niaura G. Surface-enhanced Raman spectroscopic observation of two kinds of adsorbed OH<sup>-</sup> ions at copper electrode. *Elsevier*. 2000;45:3507–3519.